SCIENTIFIC REPORTS

Correspondence and
requests for materials
should be addressed to
G.D. (duangt@issp.ac.
cn) or T.L. (tli@mail.sim.
ac.cn)

* These authors
contributed equally to
this work.

Fast-Response, Sensitivitive and Low-Powered Chemosensors by Fusing Nanostructured Porous Thin Film and IDEs-Microheater Chip

Zhengfei Dai[1]*, Lei Xu[2,3]*, Guotao Duan[1], Tie Li[2], Hongwen Zhang[1], Yue Li[1], Yi Wang[2], Yuelin Wang[2] & Weiping Cai[1]

[1]Key Lab of Materials Physics, Anhui Key lab of Nanomaterials and Nanotechnology, Institute of Solid State Physics, Chinese Academy of Sciences, Hefei, 230031, Anhui, China, [2]State Key Laboratory of Transducer Technology, and the Science and Technology on Micro-system Laboratory, Shanghai Institute of Microsystem and Information Technology, Chinese Academy of Sciences, Shanghai, 200050, China, [3]The No. 38 Research Institute, China Electronics Technology Group Corporation, Hefei 230088, China.

The chemiresistive thin film gas sensors with fast response, high sensitivity, low power consumption and mass-produced potency, have been expected for practical application. It requires both sensitive materials, especially exquisite nanomaterials, and efficient substrate chip for heating and electrical addressing. However, it is challenging to achieve repeatable microstructures across the films and low power consumption of substrate chip. Here we presented a new sensor structure via the fusion of metal-oxide nanoporous films and micro-electro-mechanical systems (MEMS)-based sensing chip. An interdigital-electrodes (IDEs) and microheater integrated MEMS structure is designed and employed as substrate chip to in-situ fabricate colloidal monolayer template-induced metal-oxide (egg. SnO_2) nanoporous sensing films. This fused sensor demonstrates mW-level low power, ultrafast response (∼1 s), and parts-per-billion lever detection for ethanol gas. Due to the controllable template strategy and mass-production potential, such micro/nano fused high-performance gas sensors will be next-generation key miniaturized/integrated devices for advanced practical applications.

C onductometric gas sensors have extensive applications in a variety of fields, such as civil life[1], envir-onment[2], food safety[3], security[4], "simple" explosive or toxic gases alarm[5] and medicine[6], particularly for detection of and monitoring far-ranging gases and vapors[7,8]. For remarkable sensitivity and excellent chemical stability, semiconducting metal oxides have been indicated as the most promising gas-sensing materials, which can easily realize irreplaceable merits of low cost, simple fabrication and good compatibility with micro-electronic processes, etc[9,10]. For conductometric gas sensors, the sensing mechanism of such gas sensors is based on the changes in electric conductance of thin film induced by interaction with the target gas-molecules[11,12]. Obviously, the sensing behavior is associated with diffusion[13] and adsorption of the target gas-molecules in the film, and their reaction with the film, which need a length of time. For the normal chemosensors, it remains to be challenge in the realization of fast response rate (within 1 s), comparatively high sensitivity, low detection limit (ppb level)[14,15]. In addition, the power consumption is high (above 100 mW) since the sensors would always working at a high temperature (250∼500°C) to achieve or activate reversible response to gases[16,17]. Till now, fabrication of gas sensors with high performances, such as fast response, high sensitivity, low power consumption, preferable stability and good selectivity, are still expected and in challenge[18,19]. Such performances should be associated directly with the surface properties, thickness and microstructures of the sensing films[20,21]. Meanwhile, the electrodes-equipped substrate for supporting sensitive materials, which is used as heating platform and electrical measurement, as well as their compatibility is also essential for the final performances[20,21].

It is well known that nanomaterials possess high surface-volume ratio, increased surface activity and strong adsorption to the target gas molecules[22,23]. So the nano-object built semiconducting films are expected to be of good gas sensing performances, and hence have been attracted much attention in the past decades. For instance, the metal-oxide semiconducting (MOS) thin films consisting of nano-objects, such as nanoparticles[24],

nanotubes[25,26], nanowires[27,28], nanorods[29,30] and hollow spheres[31], have been extensively studied in their gas-sensing properties to different gases. Generally, such nanostructured thin films display much better sensing performances than the corresponding bulk materials. However, these nanostructured porous thin films are usually produced by screen-printing or drop-coating the electrodes-equipped substrates with the slurry of preformed nano-objects. So it is difficult to control the microstructure of the film, and will thus lead to inhomogeneity in film thickness and poor reproducibility in film fabrication. In addition, the pore size in the film is uncontrollable and the film's structural stability is weak[32]. These should finally result in uncontrollability of sensing performances, and poor reliability and durability of such thin film sensors. As for the single semiconducting nanowire (or nanobelt) gas sensors, which have been widely studied[20,27,33,34], despite excellent gas sensing performance, they are unfavorable for practical application in many cases due to their complicated device construction, high cost, weak anti-jamming and large variability from sample-to-sample. Hence, a novel facile approach with low cost is highly desired in fabrication of nanostructure-based thin film gas sensors with high performances.

To solve the above problems for the MOS sensors with high performances, it is indispensable to improve both the sensing material's structures or patterns and the electrode layout in the supporting system of a device. According to our previous work[35,36], the nanostructured metal-oxide ordered pore arrays are the good candidates of the ideal sensing thin films, which are uniform and controllable in thickness, stable and tunable in microstructure, and reproducible and flexible in fabrication, due to using in-situ template techniques. Then again, the sensing thin films are mostly produced on the cylindrical or planar substrates with electrodes, usually by screen-printing[37] or drop-coating[38–40]. The resistance of the sensing devices depends on not only the film but also the distances between electrodes (or fingers), which are normally more than 200 μm. Obviously, reduction of the finger's spacing to several tens μm[16,41] or nanogaps[42,43] can pro rata decrease the detecting resistance. Meantime, the sensing film fabricated on a micromachined microhotplate platform allows quickly changing the operating temperature and smartly decreasing the heating power consumption, which can be used to rapidly regenerate the surface of the metal oxides[44]. Recently, Elmi et al. have constructed micro-machined hotplates

with circular symmetry and then achieved low power consumption with 8.9 mW at 400°C[45]; Xu et al. have reported a novel three-dimensional microheater not only with low power (30 mW at 400°C) but also gaining a very excellent heat efficiency[46]. So, if combining the template-induced ordered porous sensitive thin films with the micromachining micro-spaced inter-digital electrodes (IDEs) and microheater, we could obtain the MOS sensors with high performances, such as high sensitivity, fast response and low power consumption. However, the crucial issue is how to fabricate the well-qualified sensing layer efficiently on micro-platforms by a feasible approach.

Here, we present a flexible strategy for the chemiresistive gas sensors with high performances based on combination of structure-controllable metal oxide micro/nanostructured porous thin films and MEMS-based IDEs-microheater chip. Typically, SnO_2, the most promising gas-sensing material, is taken as the example to demonstrate the validity of this strategy. By transferring a solution-dipped self-organized colloidal template onto the stratified (sandwich) chip with micro-spaced IDEs and microheater, a SnO_2-based new gas-sensing device is fabricated. Such MEMS-assisted sensor device has exhibited the second-level response rate and 10 ppb-detectable sensitivity to ethanol, good stability and low power consumption (∼32 mW at 350°C). Also, the presented fabrication technique has favorable potential for mass production of such gas-sensing devices in batches.

Results

Figure 1a illustrates the design of the supporting system as a sandwich chip which comprises micro-spaced IDEs, isolating layer and microheater in superposing way on a SiO_2/Si_3N_4 substrate. In the chip, the micro-spaced IDEs are located on the Si_3N_4 isolating layer. Underneath is the microheater. Such chip can be fabricated by a classic MEMS technology (the details are seen in Supporting Information). Typically, Figure 1a presents a photo of the as-fabricated chip (ca. 8 mm² in area). This chip has 4 pads, two for detection of the response signal and the others for contacting the heating source.

The new sensing-device can be built by in-situ fabrication of an order porous thin film on the MEMS-based IDEs-microheater chip mat via transferring the solution-dipped organic colloidal
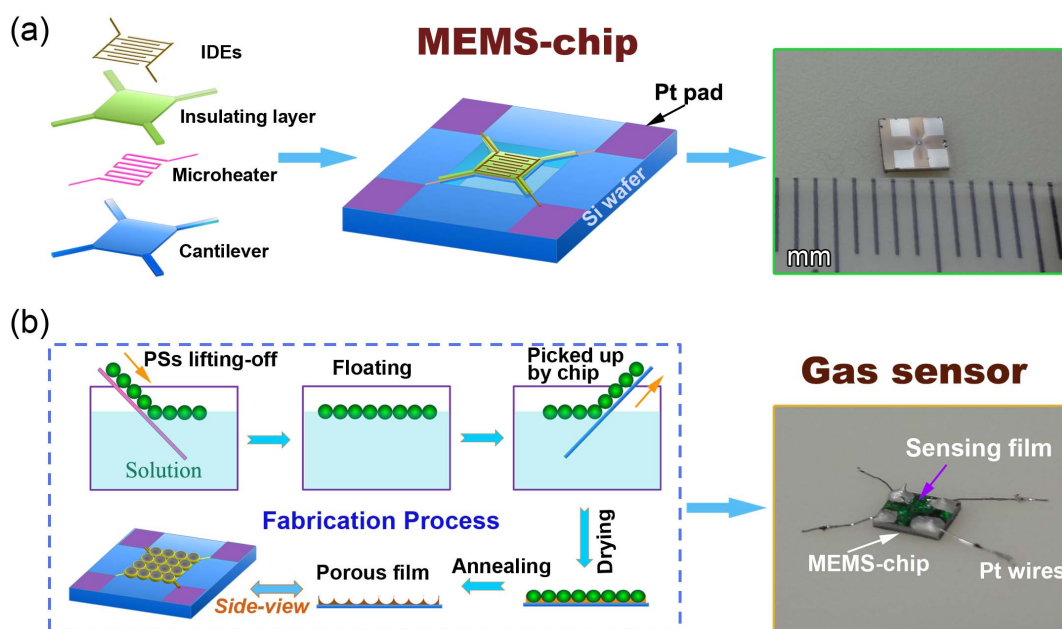

Figure 1 | Schematic illustrations and corresponding photos. (a) the MEMS-based chip structure; (b) the processing steps used to *in-situ* fabricate SnO₂ ordered porous film on an encapsulated MEMS chip.

template[32,47], as demonstrated in Figure 1b. The self-assembled polystyrene (PS) colloidal monolayer template is lifted off a glass slide and floats on the precursor solution. The floating monolayer is then transferred to the chip by picking-up. Due to the capillary effect, the monolayer on the chip also contains the precursor solution in the interstitials among colloidal spheres and between chip and monolayer. After subsequent drying and annealing, the organic colloidal template would be burnt away and the ordered porous thin film be thus formed on the IDEs-microheater chip mat due to the template geometry. Obviously, the microstructure and thickness of the thin film are controllable, depending on the size of colloidal spheres and concentration of the precursor solution. Here we take the gas-sensing material SnO_2 as an example to demonstrate the microstructure and sensing performances of such sensor. SnO_2, an n-type wide bandgap semiconductor, has been indicated as the most promising gas-sensing materials according to considerable investigations[48]. Typically, the as-fabricated gas sensor is shown in the photo of Figure 1b. The MEMS chip is covered with the SnO_2 porous thin film from 500 nm PS colloidal sphere template and annealing at 400°C, and displays greenish color originating from diffraction effect of the thin film, indicating formation of a periodic pore array. The resistance of the SnO_2 film on the chip is measured to be 120 kΩ at 25°C in air.

In addition, multi-layer ordered porous thin films can also be fabricated just by repeating the above procedures. More importantly, using the above strategy, we can easily realize the mass production of such gas sensors. Briefly, the area of the IDEs-microheater chip is about 9 mm² and the monolayer PS colloidal template can be prepared to be of more than 80 cm² in 4 inch Si wafer area (see Figure S1). As we know, the IDEs-microheater chips can be manufactured in one wafer in batches by MEMS technology. It means that we can produce about 900 gas-sensing devices by transferring a single solution-dipped wafer-scaled template onto the similarly-sized multi-chips outfitted wafer, as illustrated in Figure S2.

Figure 2 shows the morphology of the as-fabricated sensing film on IDEs-microheater chip. The working area for the IDEs-microheater chip is 150 μm × 150 μm (see Figure 2a), indicating minimization of sensor. Magnification has exhibited that the IDEs have 8 Pt fingers with 10 μm in spacing, as illustrated in Figure 2b,

corresponding to the field-emission scanning electron microscopic (FESEM) image. Obviously, such small electrode spacing will decrease the resistance value of the sensing body and hence the Johnson noise (as a square root of the resistance value)[49].

Further, we can clearly see the ordered porous SnO_2 (see phase analysis in Figure S3a) thin film which is in-situ synthesized on the IDEs, as shown in Figures 2b–d. The pores in the thin film are hexagonally arranged due to the template geometry, as shown in Figure 2c, corresponding to a high-magnification image of the sensing thin film between adjoining fingers (marked by white dot-frame Figure 2b). The thin film is highly homogenous in morphology. Further, the cross-sectional observation has shown that the porous thin film and the pore wall are about 200 nm and 20 nm in thickness, respectively, as shown in Figure S3b. Figure 2d clearly shows the continuity of the porous sensing thin film at the finger's (200 nm in thickness) edges (correspond to black dot-frame in Figure 2b) and thus an enjoyable compatibility between the nanostructured porous film with the MEMS IDEs-microheater chip. Hence, the strategy shown in Figure 1 is a good candidate for integration of the micro/nanostructured ordered porous sensing thin films on MEMS-based chips. It should be mentioned that such method is substrate-general and is suitable for the substrates not only with planar smooth surface but also with the rough and curved surface (egg. IDEs).

Discussion

The working temperature dependence on the power consumption for the sensing device has been tested. Understandably, the resistance of the Pt resistor (heater) in the sensing device is temperature-dependent. So the average temperature T (°C) of the active area in the device (marked by arrow in Figure 2a) can be determined by the resistance R of the heater, or

$$T = T_0 + \frac{R - R_0}{\alpha R_0} \qquad (1)$$

where α is the temperature first-power coefficient of Pt resistance, R_0 is the original resistance at room temperature T_0 (25°C). Obviously, by measuring the resistance of the heater under a given potential or current, the average temperature T of the active area in the device can be calculated by Eqn. (1). Figure 3 presents the heating power consumption as a function of the average temperature of the sensor, showing a nearly linear relation. If the working temperature is chosen to be T = 350°C, power consumption of the microheater is only about 32 mW, which is about 7 times lower than an excellent commercial MOS ethanol sensor (Figaro TGS2620, ca. 210 mW)[50].
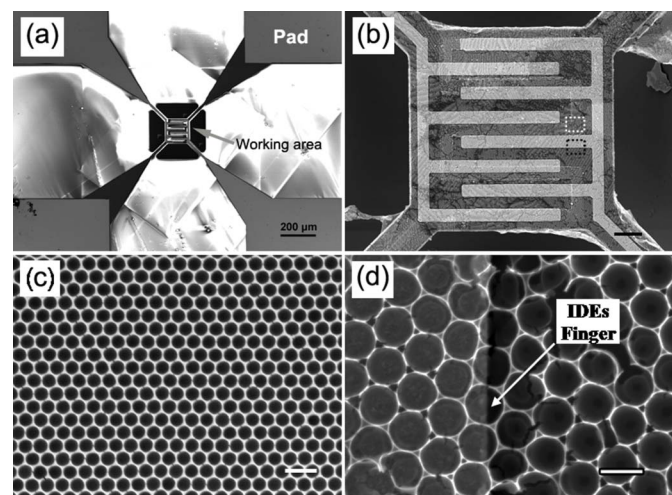

Figure 2 | The morphologies of chip and sensing porous films on the chip. (a) the top-view FESEM images of an encapsulated sandwich chip with a 150 μm × 150 μm working area; (b)- (d) FESEM images with different magnifications of a SnO_2 ordered porous films. Here (c) is a top-view image between adjoining fingers (marked by white dot-pane in b) and (d) is the top-view morphology in the junction between a finger and substrate (correspond to black dot-pane in b). The scale bars in b,c are 20 μm, and d is 500 nm.
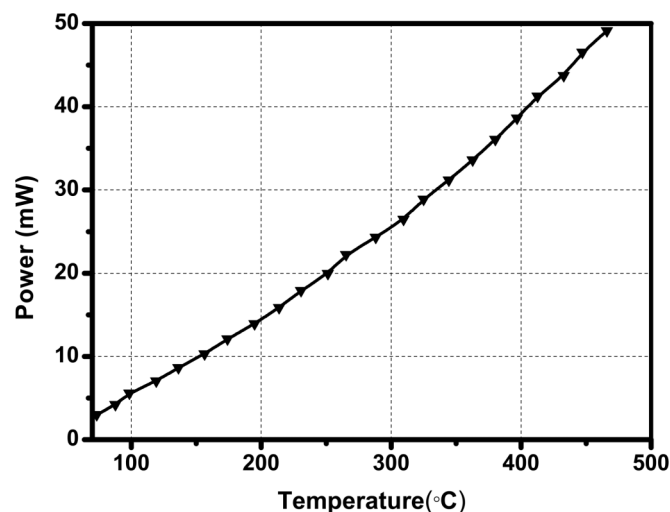

Figure 3 | The heating power (P) of the microheater as a function of working temperature (T) of the gas sensing device.

Moreover, the curve of power consumption vs. T is almost unchanged after 100 heating-cooling cycles. Such low power consumption and stability are of great significance in the practical application.

Since many semiconductor sensing materials have strong temperature dependent sensitivity and cross sensitivity, temperature gradient on the active area should be as small as possible. Based on the structure of the sensing device shown in Figure 2 and the finite-element method (FEM)[46], we can obtain the temperature distribution on the device during heating by employing electro-thermo-mechanical simulations of commercial analysis software Coventor (the simulation details are seen in SI), as typically demonstrated in Figure S4a. Corresponding to a heating power of 34 mW, the temperature on the active area is in the range of 350 to 368°C (Figure S4b and Table SI), indicating the quite homogenous temperature distribution with an average temperature gradient of about 0.2°C·μm^{-1} across the active area.

The resistance of the sensing thin film of the device in 60%RH air ambient as a function of temperature is also given in Figure S5. The resistance decreases first and then increases in the temperature range of 230 ~ 400°C. For an n-type instrinsic semiconductor, the conductivity (G) is determined by $G = nq\mu_e$, where n, q and μ_e are the carrier concentration (n $\propto$ exp(-1/T)), elementary charge and the carrier mobility, respectively[51]. The abnormal resistance increase in 230~400°C is owing to the enhanced phonon vibration (here, $\mu_e \propto T^{-3/2}$) which hinders the movement of free electrons at high temperature[51]. At 350°C, the resistance of SnO_2 film in this device is only about 135 kΩ, a relatively low resistance for the SnO_2 sensing elements in clean air comparing with other researches (~MΩ in air)[52]. This is attributed to the small finger's spacing and the parallel-connection effect of the IDEs. Hereto, it is clear that the sensing device presented in this study has merits of low power consumption and relatively homogeneous temperature distribution, and very thin and uniform sensing film with controllable structure but high-conductance.

According the previous literature[53], the average acetone concentration in exhalation from a diabetic patient is higher than 1.8 ppm, and it is necessary to distinguish the diabetic patient from a driver drinking alcohol for avoidance of misdeclaration. Here the gas sensing behaviors to ethanol and acetone are measured to demonstrate the high performances of the gas sensors presented in this study. The details of the gas-sensing measurement and setup, are described in Supporting Information, and illustrated in Figure S6. The analytes can be rapidly mixed homogenously with the background air in the cuboid chamber within 0.1s. To avoid a partial overhigh concentration (surrounding sensor) after injecting, a baffle plate is introduced with the aim to keep the concentration surrounding sensor uniform. Figure 4a presents the electric response (R_{air}/R_g) as a function of test time to ethanol under 1 ~ 5 ppm at 350°C, where R_{air} and R_g are the resistances of the sensing film in the device before and after exposure
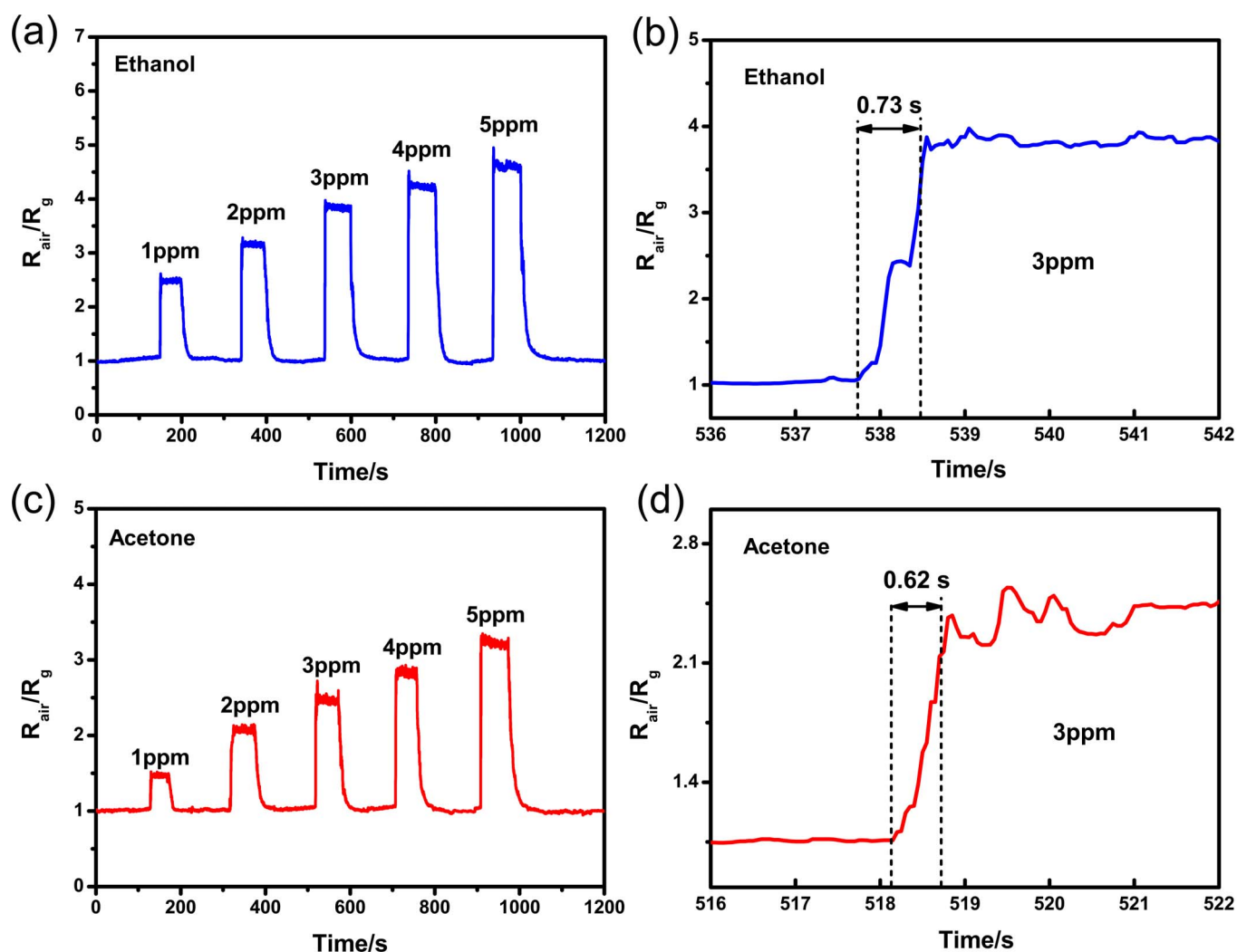

Figure 4 | The response (R_{air}/R_g) as functions of test time to ethanol and acetone. (a) to 1 ~ 5 ppm ethanol at 350°C; (b) a high magnification of (a) at 3 ppm; (c) to 1 ~ 5 ppm acetone at 350°C and (d) a high magnification of (c) at 3 ppm, respectively.

to the target gases, respectively. Here the sensor signal S is defined as R_{air}/R_{g0} where R_{g0} is the stable or minimal resistance after exposure to the test gas. The as-fabricated sensors exhibit a high sensing signal and ultrafast response, as shown in Figures 4a and b. With the exposure to 3 ppm ethanol, for example, the signal is about 3.9 and the response time is less than 1s (0.73 s). Herein, the response-time is defined as the time taken for the sensor-output to reach 90% of its steady value[9]. The resistance of the sensing body at 350°C is about 30 kΩ in 5 ppm EtOH ambient, which is beneficial to possess low noise for trace detection. Similarly, the sensing performance to acetone at 350°C is also observed, as illustrated in Figures 4c and d. The signal and response time are 2.5 and 0.62 s respectively, under 3 ppm acetone. Further, we have repeated the sensing tests using another five MEMS-based sensors fabricated by the same procedure, showing in Figure S7. Under 350°C (32 mW on microheater) and 60%RH, such sensors' signals have displayed a good repeatability. The response time for the previously reported MOS gas sensors is usually in the range of several ten-seconds to minutes. For the sensor in this study, however, it is less than 1 second. In n-type oxide semiconductors, the sensing response interaction to reducing gas involves in-diffusion of target gas onto the sensing body surface and subsequently oxidation by negative charged adsorbed oxygens, i.e. O^- or O^{2-}. The rapid response indicates that the diffusion and its oxidation with O^- or O^{2-} occur very speedily in our porous structures. In our case, about 5 nm grain size (see the inset of Figure S3b) is smaller than two times of Debye length of pure SnO_2 (ca. 3 nm at 250°C)[54], suggesting a grain self-controlled sensing behavior. Theoretically, grain sizes exceed twice the Debye length will be unfavorable to the overall conductance change of the sensitive materials, and vice versa[55]. As for the fast response, it may be mainly attributed to the porous and ultra-thin (20 nm) structure of the film (Figure 2c,d and Figure S2a.). Such structure induces easy and fast accessibility to all the film's surface for the target gases after exposure[56].

A low determination limit is important for the gas sensors in trace or ultratrace target gas analysis[57]. Figure 5 shows the sensing results when exposure to the sub-ppm ethanol gas. To observe the sensor response to 100 ppb ethanol in ambient gas which even contains low-concentration ethanol, a continuous test without recoveries was taken in the concentration range from 100 ppb to 500 ppb at 350°C. In this condition, the response time and sensing signal is, respectively, about 1.2 s and 1.1 to 100 ppb ethanol. Further, the dependence of the sensing signal on the concentration of the target gases has been obtained. Such dependence can be well described by the empirical equation from MOS gas sensors[58]

$$S = AC^\beta + 1 \qquad (2)$$

where A is the constant, C the concentration of the target gas with the unit of ppm. The power exponent β is the parameter (usually from 0.5 to 1) depending on the charge of the surface species and the stoichiometry of the elementary reactions on the surface. The sensing signal as a function of the concentration is illustrated in the inset of Figure 5, and a linear dependence in the sub-ppm range is addressed (Eqn.3), with the aim to predict the potential detection limits.

$$S = 1.0 + 0.89 \times C \qquad (3)$$

Interestingly, our sensor displays a strong resolving power to low-concentration ethanol, due to the low noise in the testing process. Obviously, if there is no noise, an extremely slight change of the acquired signal can confirm the existence of a gas when the ambient atmosphere is unchanged. Here, the detectable lower limit of the test gas concentration can be reasonably predicted on basis of the present signal-to-noise ratio. In Figure 5b, the noise signal N is observed to be about 0.01 in scale. The standard requirement of the detection limit is $(S-1)/N > 3$ [59]. So, the response signal should be larger than 0.03 or the value of the sensing signal must be >1.03. From the Eqn. (3), the corresponding concentration can be estimated to be about 30 ppb with a signal of 1.03 when the drift of the sensor baseline is significantly lower. It means that the detectable lower limit of concentration to ethanol is about 30 ppb at 350°C. This detectable limit is quite low compared with the recently reported results in literatures, such as 50 ppb on orthorhombic $ZnO \cdot SnO_2$ nanosheets based sensor[52]. In addition, this detectable limit even gets close to that of different single nanowires (or nanobelts) whose gas sensing behaviors have been widely studied[27]. However, the construction of single-nanowire sensing devices demands complicated manipulation, and it also traps in high cost, weak anti-jamming capability and non-uniformity of individual nanowire.

The dependence of sensing signal on the working temperature was also examined. Figures 6a and b present the corresponding results for our as-fabricated sensor exposed to ethanol and acetone, respectively, in the concentration range of 1–5 ppm. It is found that the highest response temperatures for ethanol and acetone are 350°C and 400°C at 60%RH ambient, respectively. For semiconducting metal oxide gas sensors, the optimal operation temperature is generally influenced by the sensing materials, gas species, doping or surface modification, synthesized routes and microstructures[60–62]. The highest response temperature about 350°C to ethanol is also reported by other literatures[63]. In the 60%RH atmosphere background, such highest response working temperatures are independent of the gas-concentrations. This indicates that we may realize a selective detection by using multi-sensors with similar structures while working at different temperature. Further and deep study about this issue is still in progress.

We further investigated the stability and the effect of ambient on the sensors. Figure S8 shows the long term stability (half one year) of the as-fabricated sensors. The sensing signal only exhibits a small decrease from 4.67 to 4.12 in half one year under 350°C and 60%RH, indicating a good long-term stability. To investigate the effect from ambient, we have observed the EtOH-sensing (5 ppm, 350°C) performance at different ambient conditions, as shown in Figure S9. The sensor signal ranges from 4.2 at 20%RH to 4.8 at 80%RH. Comparing with the EtOH, the effect of the ambient humidity on sensor response is relatively low.

Further considering TWA (time weighted average) for real applications, the EtOH sensing was measured in the 100~500 ppm range at 350°C and 60%RH (Figure S10). The sensing signals are about 23 and 27 corresponding to 100 and 500 ppm EtOH, respectively. It shows that the sensing signal reach saturation in the higher concentration content. This indicates that the as-prepared sensors be more
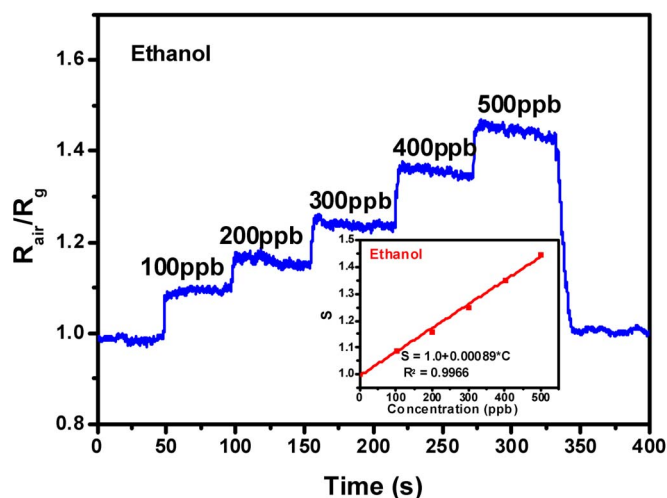

Figure 5 | A continuous test without recoveries to 100-500 ppb ethanol concentration range at 350°C. The inset is the corresponding sensing signal vs. gas concentration linear fitting curve.
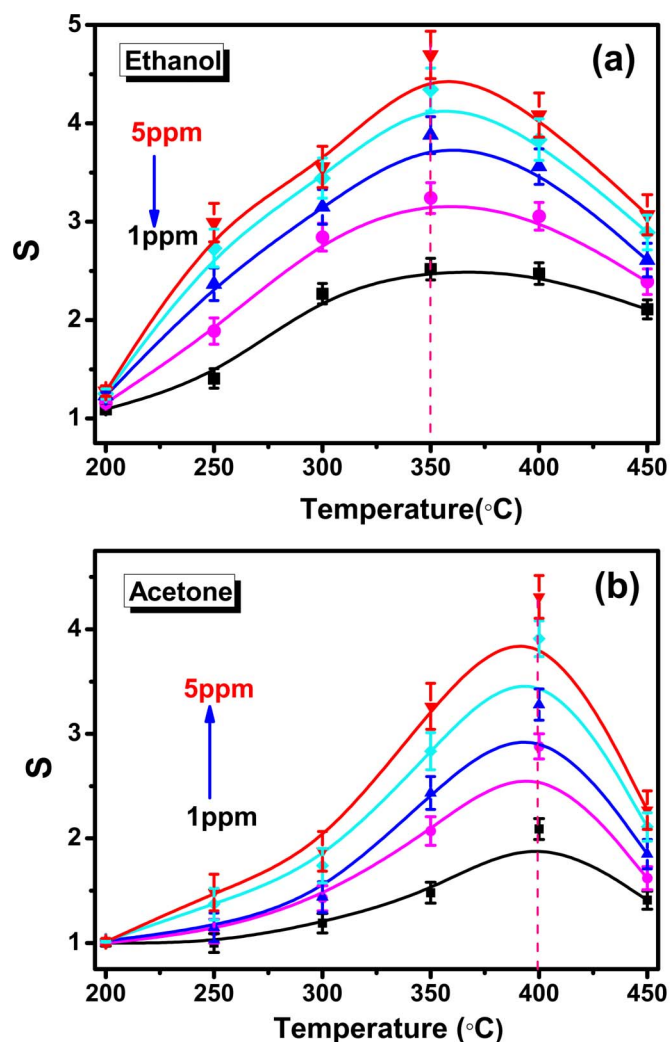
Figure 6 | The sensing signal vs.temperature curves to (a) ethanol and (b) acetone. Different colors represent the gas of 1,2,3,4 and 5 ppm.

suitable for detection in low concentration range. Comparing the results to those in literatures, it can found the sensitivity in our case is higher than those from Sr-doped nanostructured LaFeO₃ film and sol-gel derived ZnO thin film[60,62], and close to that from ultrathin InN field-effect transistors[61]. However, the response time is smaller than that from InN field-effect transistors[61].

In summary, we present a flexible strategy for the chemiresistive gas sensors with high sensitivity, fast response and low power con-sumption, based on combination of nanostructured metal-oxide ordered porous thin films and micro-spaced interdigital electrodes chip. By transferring the solution-dipped self-organized PS colloidal template onto a MEMS-based chip, we can realize such combination and achieve the new gas sensor with high performances. Importantly, this fabrication strategy is suitable for mass production of such gas-sensing devices and about 900 ones could be produced in each batch. Representatively, the sensing material SnO₂ is taken as the example and the structure-controllable SnO₂ ordered porous thin film is thus *in-situ* fabricated on the sandwich chip to form a gas senor. Due to the special structure, such devices have exhibited fast response within 1 s, mW-level low power-consumption (~30 mW), sensitivity to EtOH and acetone (30 ppb-detectable limit to ethanol), high stability, good fabrication repeatability and potential in low-cost mass produc-tion. This could be an important progress in the chemiresitive thin film gas sensors and an important step toward their practical applica-tions in some advanced fields where the high sensitivity, fast response

and low power consumption are simultaneously needed. This study also provides a new way for design and fabrication of the resistance-typed gas sensors with high performances.

Methods

Fabrication of the supporting system. The supporting chips with the IDEs and microheater were fabricated by a classic MEMS process (see Supporting Information). Briefly, a 150 μm × 150 μm SiO₂ (400 nm in thickness)/Si₃N₄ (600 nm in thickness) membrane was successively deposited on an N-type <100> oriented silicon wafer. A serpentine Pt/Ti resistor on the membrane was linked to the bulk silicon slice via four slender cantilever beams. Then an isolated layer Si₃N₄ (600 nm in thickness) was deposited above them. Subsequently, Pt IDEs (8 fingers, 100 μm in length, 10 μm in width and 10 μm in spacing) were patterned on this Si₃N₄ layer. Thus, a Pt-IDEs/Si₃N₄/microheater sandwich chip on the SiO₂/Si₃N₄ substrate with a silicon wafer encapsulated in their bottom was fabricated.

Integration of gas-sensing device. The SnO₂ ordered porous thin film-gas sensing devices were fabricated by transferring the solution-dipped self-organized PS colloidal template onto the above sandwich chip, as illustrated in Figure 1b. Firstly, an ordered PS colloidal monolayer template, with the sphere diameter of 500 nm, was prepared by air/water interfacial assembly[47]. Such a monolayer on the glass substrate was integrally lifted off by aslant dipping into a 0.1 M SnCl₄ precursor solution in a beaker due to surface tension of the solution and then floated on the solution surface. In succession, the floating PS colloidal monolayer was picked up with the encapsulated sandwich chip and dried at 120 °C for 0.5 h. After it was subsequently heated at 400°C for 2 h, the PS template was burned away, an ordered porous SnO₂ thin film was formed on the chip, and thus the new gas sensor, integrating micro/ nanostructured porous thin film with IDE-microheater-chip, was fabricated.

Structural characterization. The morphologies and microstructures of the samples were examined on a field-emission scanning electron microscope (FESEM, Sirion 200) and a transmission electron microscope (TEM H-800). Phase analysis of the films was carried out on a Philips X'Pert powder X-ray diffractometer using Cu Kα (0.15419 nm) radiation. The optical photographs of the electrode and the sensing films were obtained using a digital camera (Sony DSC-WX9).

Measurement of gas sensing performances. The gas sensing experiments were carried out in a static system (a cuboid chamber with the size of 30 cm × 30 cm × 20 cm, see Figure S6) with a multimeter/DC power supply (Agilent mod. U3606A and U8002A) by measuring the electrical voltage evolutions of sensing devices. A certain amount of ethanol-saturated and acetone-saturated vapor was injected into the gas-chamber with sample in the system. The ethanol concentration in the chamber can be calculated based on the injected amount. With Labview software, the heating voltage was controlled and data were acquired. All the measurements were carried out in the 25°C air ambient. The working temperatures of sensors are no more than 450°C to earn a longer lifetime of sensors, owing to a breakage of Pt microheater possibly occurring at a higher working temperature (such as 500°C).

1. Collins, P. G., Bradley, K., Ishigami, M. & Zettl, A. Extreme oxygen sensitivity of electronic properties of carbon nanotubes. *Science* **287**, 1801–1804 (2000).
2. Modi, A., Koratkar, N., Lass, E., Wei, B. Q. & Ajayan, P. M. Miniaturized gas ionization sensors using carbon nanotubes. *Nature* **424**, 171–174 (2003).
3. Peres, L. O., Li, R. W. C., Yamauchi, E. Y., Lippi, R. & Gruber, J. Conductive polymer gas sensor for quantitative detection of methanol in Brazilian sugar-cane spirit. *Food Chem.* **130**, 1105–1107 (2012).
4. Gourine, A. V., Llaudet, E., Dale, N. & Spyer, K. M. ATP is a mediator of chemosensory transduction in the central nervous system. *Nature* **436**, 108–111 (2005).
5. Rock, F., Barsan, N. & Weimar, U. Electronic nose: Current status and future trends. *Chem. Rev.* **108**, 705–725 (2008).
6. Zhao, D. *et al.* Surface Functionalization of Porous Coordination Nanocages Via Click Chemistry and Their Application in Drug Delivery. *Adv. Mater.* **23**, 90–93 (2011).
7. Liu, N., Tang, M. L., Hentschel, M., Giessen, H. & Alivisatos, A. P. Nanoantenna-enhanced gas sensing in a single tailored nanofocus. *Nat. Mater.* **10**, 631–636 (2011).
8. Yavari, F. *et al.* High Sensitivity Gas Detection Using a Macroscopic Three-Dimensional Graphene Foam Network. *Sci. Rep.* **1**, 166 (2011).
9. Franke, M. E., Koplin, T. J. & Simon, U. Metal and metal oxide nanoparticles in chemiresistors: Does the nanoscale matter? *Small* **2**, 36–50 (2006).
10. Kuang, Q., Lao, C. S., Wang, Z. L., Xie, Z. X. & Zheng, L. S. High-sensitivity humidity sensor based on a single SnO2 nanowire. *J. Am. Chem. Soc.* **129**, 6070–6071 (2007).
11. Batzill, M. & Diebold, U. The surface and materials science of tin oxide. *Prog. Surf. Sci.* **79**, 47–154 (2005).
12. Yamazoe, N., Sakai, G. & Shimanoe, K. Oxide semiconductor gas sensors. *Catal. Surv. Asia* **7**, 63–75 (2003).
13. Sakai, G., Matsunaga, N., Shimanoe, K. & Yamazoe, N. Theory of gas-diffusion controlled sensitivity for thin film semiconductor gas sensor. *Sensor.Actuat. B-Chem.* **80**, 125–131 (2001).

14. McAlpine, M. C., Ahmad, H., Wang, D. & Heath, J. R. Highly ordered nanowire arrays on plastic substrates for ultrasensitive flexible chemical sensors. *Nat. Mater.* **6**, 379–384 (2007).

15. Chen, G., Paronyan, T. M., Pigos, E. M. & Harutyunyan, A. R. Enhanced gas sensing in pristine carbon nanotubes under continuous ultraviolet light illumination. *Sci. Rep.* **2**, 343 (2012).

16. Hubner, M. *et al.* The Structure and Behavior of Platinum in SnO(2)-Based Sensors under Working Conditions. *Angew. Chem. Int. Edit.* **50**, 2841–2844 (2011).

17. Potje-Kamloth, K. Semiconductor junction gas sensors. *Chem. Rev.* **108**, 367–399 (2008).

18. Korotcenkov, G. Metal oxides for solid-state gas sensors: What determines our choice? *Mat. Sci. Eng. B-Solid* **139**, 1–23 (2007).

19. Stetter, J. R. & Li, J. Amperometric gas sensors - A review. *Chem. Rev.* **108**, 352–366 (2008).

20. Pearton, S. J. *et al.* Recent advances in wide bandgap semiconductor biological and gas sensors. *Prog. Mater. Sci.* **55**, 1–59 (2010).

21. Tricoli, A., Righettoni, M. & Teleki, A. Semiconductor Gas Sensors: Dry Synthesis and Application. *Angew. Chem. Int. Edit.* **49**, 7632–7659 (2010).

22. Kolmakov, A. & Moskovits, M. Chemical sensing and catalysis by one-dimensional metal-oxide nanostructures. *Annu. Rev. Mater. Res.* **34**, 151–180 (2004).

23. Heo, Y. W. *et al.* ZnO nanowire growth and devices. *Mat. Sci. Eng. R* **47**, 1–47 (2004).

24. Cao, M., Wang, Y., Chen, T., Antonietti, M. & Niederberger, M. A Highly Sensitive and Fast-Responding Ethanol Sensor Based on CdIn2O4 Nanocrystals Synthesized by a Nonaqueous Sol−Gel Route. *Chem. Mater.* **20**, 5781–5786 (2008).

25. Rocha, A. R., Rossi, M., Fazzio, A. & da Silva, A. J. R. Designing real nanotube-based gas sensors. *Phys. Rev. Lett.* **100**, 176803 (2008).

26. Du, N. *et al.* Porous indium oxide nanotubes: Layer-by-layer assembly on carbon-nanotube templates and application for room-temperature NH3 gas sensors. *Adv. Mater.* **19**, 1641–1645 (2007).

27. Mai, L. Q. *et al.* Single beta-AgVO(3) Nanowire H(2)S Sensor. *Nano Lett.* **10**, 2604–2608 (2010).

28. Liu, B. *et al.* Hierarchical Three-Dimensional ZnCo2O4 Nanowire Arrays/Carbon Cloth Anodes for a Novel Class of High-Performance Flexible Lithium-Ion Batteries. *Nano Lett.* **12**, 3005–3011 (2012).

29. Li, C. C. *et al.* Surface-depletion controlled gas sensing of ZnO nanorods grown at room temperature. *Appl. Phys. Lett.* **91**, 032101 (2007).

30. Huang, H. *et al.* Low-Temperature Growth of SnO(2) Nanorod Arrays and Tunable n-p-n Sensing Response of a ZnO/SnO(2) Heterojunction for Exclusive Hydrogen Sensors. *Adv. Funct. Mater.* **21**, 2680–2686 (2011).

31. Xu, H. L. & Wang, W. Z. Template synthesis of multishelled Cu2O hollow spheres with a single-crystalline shell wall. *Angew. Chem. Int. Edit.* **46**, 1489–1492 (2007).

32. Jia, L. C. & Cai, W. P. Micro/Nanostructured Ordered Porous Films and Their Structurally Induced Control of the Gas Sensing Performances. *Adv. Funct. Mater.* **20**, 3765–3773 (2010).

33. Baik, J. M. *et al.* Pd-Sensitized Single Vanadium Oxide Nanowires: Highly Responsive Hydrogen Sensing Based on the Metal-insulator Transition. *Nano Lett.* **9**, 3980–3984 (2009).

34. Sysoev, V. V. *et al.* Single-Nanobelt Electronic Nose: Engineering and Tests of the Simplest Analytical Element. *ACS Nano* **4**, 4487–4494 (2010).

35. Li, Y., Cai, W. & Duan, G. Ordered micro/nanostructured arrays based on the monolayer colloidal crystals. *Chem. Mater.* **20**, 615–624 (2008).

36. Jia, L. C., Cai, W. P., Wang, H. Q., Sun, F. Q. & Li, Y. Hetero-apertured Micro/Nanostructured Ordered Porous Array: Layer-by-Layered Construction and Structure-Induced Sensing Parameter Controllability. *ACS Nano* **3**, 2697–2705 (2009).

37. Fan, Z. Y. *et al.* Toward the Development of Printable Nanowire Electronics and Sensors. *Adv. Mater.* **21**, 3730–3743 (2009).

38. Zhang, H. G. *et al.* One-pot synthesis and hierarchical assembly of hollow Cu2O microspheres with nanocrystals-composed porous multishell and their gas-sensing properties. *Adv. Funct. Mater.* **17**, 2766–2771 (2007).

39. Liu, X. H., Zhang, J., Guo, X. Z., Wu, S. H. & Wang, S. R. Amino acid-assisted one-pot assembly of Au, Pt nanoparticles onto one-dimensional ZnO microrods. *Nanoscale* **2**, 1178–1184 (2010).

40. Wang, C. X. *et al.* Large Scale Synthesis and Gas-Sensing Properties of Anatase TiO(2) Three-Dimensional Hierarchical Nanostructures. *Langmuir* **26**, 12841–12848 (2010).

41. Jimenez-Cadena, G., Riu, J. & Rius, F. X. Gas sensors based on nanostructured materials. *Analyst* **132**, 1083–1099 (2007).

42. Lee, J., Shim, W., Lee, E., Noh, J.-S. & Lee, W. Highly Mobile Palladium Thin Films on an Elastomeric Substrate: Nanogap-Based Hydrogen Gas Sensors. *Angew. Chem. Int. Edit.* **50**, 5301–5305 (2011).

43. Covington, E., Bohrer, F. I., Xu, C., Zellers, E. T. & Kurdak, C. Densely integrated array of chemiresistor vapor sensors with electron-beam patterned monolayer-protected gold nanoparticle interface films. *Lab Chip* **10**, 3058–3060 (2010).

44. Ruiz, A. M., Illa, X., Diaz, R., Romano-Rodriguez, A. & Morante, J. R. Analyses of the ammonia response of integrated gas sensors working in pulsed mode. *Sensor. Actuat. B-Chem.* **118**, 318–322 (2006).

45. Elmi, I., Zampolli, S., Cozzani, E., Mancarella, F. & Cardinali, G. C. Development of ultra-low-power consumption MOX sensors with ppb-level VOC detection capabilities for emerging applications. *Sensor. Actuat. B-Chem.* **135**, 342–351 (2008).

46. Lei, X., Tie, L. & Yuelin, W. A Novel Three-Dimensional Microheater. *IEEE Electr. Device L.* **32**, 1284–1286 (2011).

47. Dai, Z., Li, Y., Duan, G., Jia, L. & Cai, W. Phase Diagram, Design of Monolayer Binary Colloidal Crystals, and Their Fabrication Based on Ethanol-Assisted Self-Assembly at the Air/Water Interface. *ACS Nano* **6**, 6706–6716 (2012).

48. Comini, E. *et al.* Quasi-one dimensional metal oxide semiconductors: Preparation, characterization and application as chemical sensors. *Prog. Mater. Sci.* **54**, 1–67 (2009).

49. Schedin, F. *et al.* Detection of individual gas molecules adsorbed on graphene. *Nat. Mater.* **6**, 652–655 (2007).

50. Figaro Engineering Inc: Products, Gas senors. http://www.figaro.co.jp/en/product/indexphp?mode=search&kbn=1&type=30&id=213010.

51. Grundmann, M. The Physics of Semiconductors: An Introduction Including Devices and Nanophysics. *Springer, Heidelberg* (2006).

52. Chen, Y. *et al.* An evolution from 3D face-centered-cubic ZnSnO3 nanocubes to 2D orthorhombic ZnSnO3 nanosheets with excellent gas sensing performance. *Nanotechnology* **23**, 415501 (2012).

53. Owen, O. E. *et al.* Acetone Metabolism during Diabetic-Ketoacidosis. *Diabetes* **31**, 242–248 (1982).

54. Xu, C., Tamaki, J., Miura, N. & Yamazoe, N. Grain-Size Effects On Gas Sensitivity of Porous SnO2-Based Elements. *Sensor. Actuat. B-Chem.* **3**, 147–155 (1991).

55. Tiemann, M. Porous metal oxides as gas sensors. *Chem-Eur. J.* **13**, 8376–8388 (2007).

56. Yamazoe, N. & Shimanoe, K. Roles of shape and size of component crystals in semiconductor gas sensors. *J. Electrochem. Soc.* **155**, J85–J92 (2008).

57. Ishikawa, F. N. *et al.* Label-Free, Electrical Detection of the SARS Virus N-Protein with Nanowire Biosensors Utilizing Antibody Mimics as Capture Probes. *ACS Nano* **3**, 1219–1224 (2009).

58. Scott, R. W. J. *et al.* Tin dioxide opals and inverted opals: Near-ideal microstructures for gas sensors. *Adv. Mater.* **13**, 1468–1472 (2001).

59. Kim, I. D., Rothschild, A., Hyodo, T. & Tuller, H. L. Microsphere templating as means of enhancing surface activity and gas sensitivity of CaCu3Ti4O12 films. *Nano Lett.* **6**, 193–198 (2006).

60. Murade, P. A., Sangawar, V. S., Chaudhari, G. N., Kapse, V. D. & Bajpeyee, A. U. Acetone gas-sensing performance of Sr-doped nanostructured LaFeO3 semiconductor prepared by citrate sol–gel route. *Curr. Appl. Phys.* **11**, 451–456 (2011).

61. Kao, K. W., Hsu, M. C., Chang, Y. H., Gwo, S. & Yeh, J. A. A sub-ppm acetone gas sensor for diabetes detection using 10 nm thick ultrathin InN FETs. *Sensors (Basel)* **12**, 7157–7168 (2012).

62. Kakati, N., Jee, S. H., Kim, S. H., Oh, J. Y. & Yoon, Y. S. Thickness dependency of sol-gel derived ZnO thin films on gas sensing behaviors. *Thin Solid Films* **519**, 494–498 (2010).

63. Zhang, Y., Li, J. P., An, G. M. & He, X. L. Highly porous SnO(2) fibers by electrospinning and oxygen plasma etching and its ethanol-sensing properties. *Sensor. Actuat. B-Chem.* **144**, 43–48 (2010).

Acknowledgments

Author contributions

G.D. and T.L. initiated the work; G.D., T.L. and W.C. supervised the work; Z.D. carried out the gas sensing lab on an IDEs-microheater chip based on nanostructured porous thin film; L.X. designed IDEs-microheater chip and made out the FEM imulation; Y.L. helped to fabricate themonolayer colloidal template via ethanol-assisted self-assembly; H.Z. took the photograph and scanning electron microscope images; Y.W. machined IDEs-microheater chip by MEMS. All authors discussed the results and commented on the manuscript.

Additional information

How to cite this article: Dai, Z. *et al.* Fast-Response, Sensitivitive and Low-Powered Chemosensors by Fusing Nanostructured Porous Thin Film and IDEs-Microheater Chip. *Sci. Rep.* **3**, 1669; DOI:10.1038/srep01669 (2013).